# Mixing in Coaxial Confined Jets of Large Velocity Ratio

M.M.C.L. Lima[(1)†] and J.M.L.M. Palma[(2)‡]

Faculdade de Engenharia da Universidade do Porto
Rua Dr. Roberto Frias s/n
4200-465 Porto, Portugal

[(1)] E-mail: mmlima@civil.uminho.pt
[(2)] E-mail: jpalma@fe.up.pt

**ABSTRACT**

Simultaneous measurements of velocity and concentration in coaxial jets, confined by a cylindrical duct (figure 1), were made by a combined Laser Doppler Velocimetry/Laser Induced Fluorescence technique. A fluorescent tracer was added to the inner jet, to study the mixing for two velocity ratios between the mean axial velocities of annular ($U_a$) and inner flows ($U_{in}$) equal to 3.2 and 6.5, and Reynolds numbers of about $3\times10^4$, based on the bulk velocity and inner diameter of the outer tube ($D$).

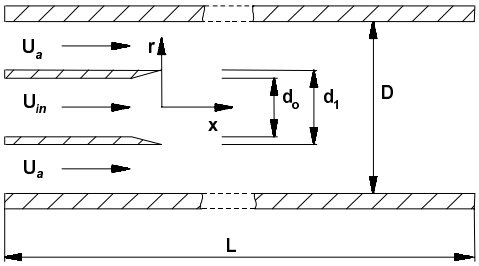


*Fig. 1. Flow configuration ($d_0$ = 17 mm, $d_1$ = 19 mm, D = 42 mm, L = 2000 mm)*

From the analysis of mean and instantaneous velocity and concentration fields, we concluded that mixture was enhanced as the velocity ratio increased from 3.2 to 6.5, showing the dependence between mixture and the intensity of the shear layer between the two flows. The topology of the mean velocity field was different between the two cases; for higher velocity ratio of 6.5 a recirculation region prevailed at a distance of 1 inner diameter ($d_0$) from the jet outlet, with consequences on the jets near field.

One of the objectives of the current study was the characterization and analysis of the passive scalar transport by the turbulent field, given its importance in many engineering systems. The paper includes flow visualization, axial and radial turbulent scalar fluxes, higher order moments and single and joint probability density functions of both velocity and scalar fields.

† Current address: Escola de Engenharia da Universidade do Minho, Campus de Azurém, 4800-058 Guimarães, Portugal
‡ Corresponding author.

## 1. INTRODUCTION

In spite of the advances in the development of computational methods, the study of turbulence remains accessible only by experimentation, namely for high Reynolds numbers (cf., Bradshaw, 1994). The simultaneous measurements of velocity and concentration fields permit the verification of diffusive transport hypothesis and the determination of turbulent flux of mass, which are essential for mathematical modelling of turbulent mass transport, common in engineering applications and in the atmospheric boundary layer.

Coaxial jets, which have been studied for 30 years now (eg, Champagne and Wygnansky (1971), Johnson and Bennett (1981), Villermaux and Rehab (2000)), are a flow of great interest because of the variety of phenomena that they can provide (eg,, turbulent shear layers interaction, vortex shedding, recirculation) and their practical relevance, with applications in many engineering devices, such as combustion chambers, injection systems, etc..

For Reynolds numbers high enough (between $10^3$ and $10^4$) the main parameter that influences the flow and determines its evolution is the ratio between the momentum of the annular and inner flows, $\rho_a U_a^2/\rho_{in} U_{in}^2$ (Rehab et al., 1997), i.e. the velocity ratio $U_a/U_{in}$ in case of uniform density flows ($\rho_a = \rho_{in}$), which can be also understood as the shear layer intensity $|U_a/U_{in} -1|$. Rehab et al. (1998) study the influence of flow geometry, such as inner and annular jets area ratio, inner jet tube wall thickness and shape of velocity profiles at the inlet section. Villermaux and Rehab (2000) suggest that in coaxial jets with outer to inner velocity ratio higher than unity, the two parameters controlling the mixing process are the initial vorticity thickness $\delta \sim (D-d_1)\, Re^{-1/2}$ of the outer, fast stream, and the elongation rate $\gamma = 2\,(U_a - U_{in})/(D-d_1)$, based on the velocity difference between the two streams and the gap thickness of the annular jet.

The present paper differs from many previous studies available in the published literature, because coaxial jets are not discharged into stagnant fluid, where the flow evolves into a single jet type, after the merging of the annular and inner flows. Here, a tube, cylindrical, wall confines the two co-flowing jets and this may affect not only the flow final stage, but also the jets near field to an extent to be determined by the measurements.

The experimental set-up and measuring equipment are described in the following section. The results and their discussion are presented in Section 3, including mean and turbulent velocity and concentration fields, turbulent mass transport, and visualization and probability density functions analysis. Section 4 is the final section, with the main conclusions.

## 2. EXPERIMENTAL SET-UP

### Geometry

The flow geometry (figure 1) was made of 2 coaxial water flows enclosed in a cylindrical duct constructed from Perspex. The test section was 2 m long (42 mm internal diameter) with optical access made through an optical box, filled in with water to reduce refraction effects. A solution of rhodamine B of known concentration was injected in the inner jet water circuit by an electronic diaphragm-metering pump (Cole Parmer G74110-15), resulting in a jet flow of water and rhodamine B (Arcoumanis et al., 1990) in a concentration of 0.04 mg/L.

### Optical set-up

The light source was an argon-ion laser (Spectra-Physics, Stabilite 2017) operating in power stability mode at 514.5 nm. The optical system consisted of a conventional one-component laser Doppler Dantec 55× modular optics, with a ±40 MHz Bragg cell (frequency shifter, Dantec 55N11) and a 310 mm front lens. A colour separator split the collected light into 2 wavelengths, above and below 590 nm, which were filtered before reaching the corresponding photo multipliers for velocity (514.5 nm interference filter, Dantec 55×37) and concentration (high pass filter, OG570 Melles Griot) signals.

### Data-processing

LDV data processing was performed using a TSI Counter (1990C) operated at single measurement per burst mode (SM/B), for a 1% comparison between frequencies, estimated with 8 and 5 measurement cycles. Data acquisition was performed using a velocimetry board Zechs Electronics (1400A) together

with an Analog Digital Converter module, interfaced to the computer. Both signals (velocity and concentration) were acquired simultaneously, whenever the counter validated velocity.

For flow visualization, the argon-ion laser was used at its highest power (1.8 W) and a set of still images were obtained at shutter speeds of 1/8000 s, i.e. an integration time of 125 μs.

A more detailed description of the test rig, measuring equipment and experimental methodology, including uncertainty analysis, can be found in a companying paper in the current proceedings, Lima et al. (2002), and also in the doctoral thesis of Lima (2000).

## 3. RESULTS

The flow was studied (Table 1) for velocity ratios $U_a/U_{in}$ equal to 3.2 and 6.5, between the mean axial velocities of annular ($U_a$) and internal flows ($U_{in}$), and Reynolds numbers in the order of $3\times10^4$, based on the bulk velocity and inner diameter of the outer tube.

*Table 1. Experimental flow conditions*

| N. | $U_a/U_{in}$ | $U_a$ | $Re_a$ | $U_{in}$ | $Re_{in}$ | $\lvert U_a/U_{in}-1\rvert$ | $Re_{bulk}$ |
|---|---|---|---|---|---|---|---|
| 1 | 3.2 | 0.83 | 9450 | 0.26 | 4376 | 2.2 | $2.923\times10^4$ |
| 2 | 6.5 | 0.83 | 9450 | 0.13 | 2134 | 5.5 | $2.832\times10^4$ |

$U_a$: average axial velocity in the annulus [$ms^{-1}$];
$U_{in}$: average axial velocity at the outlet of the inner tube [$ms^{-1}$];
$Re_a$: Reynolds number based on $U_a$ and size of the annular gap;
$Re_{in}$: Reynolds number based on $U_{in}$ and $d_0$
$Re_{bulk}$: Reynolds number based on $U_{bulk}$ and $D$

### 3.1 Mean and Turbulent Velocity and Concentration Fields along the Centreline

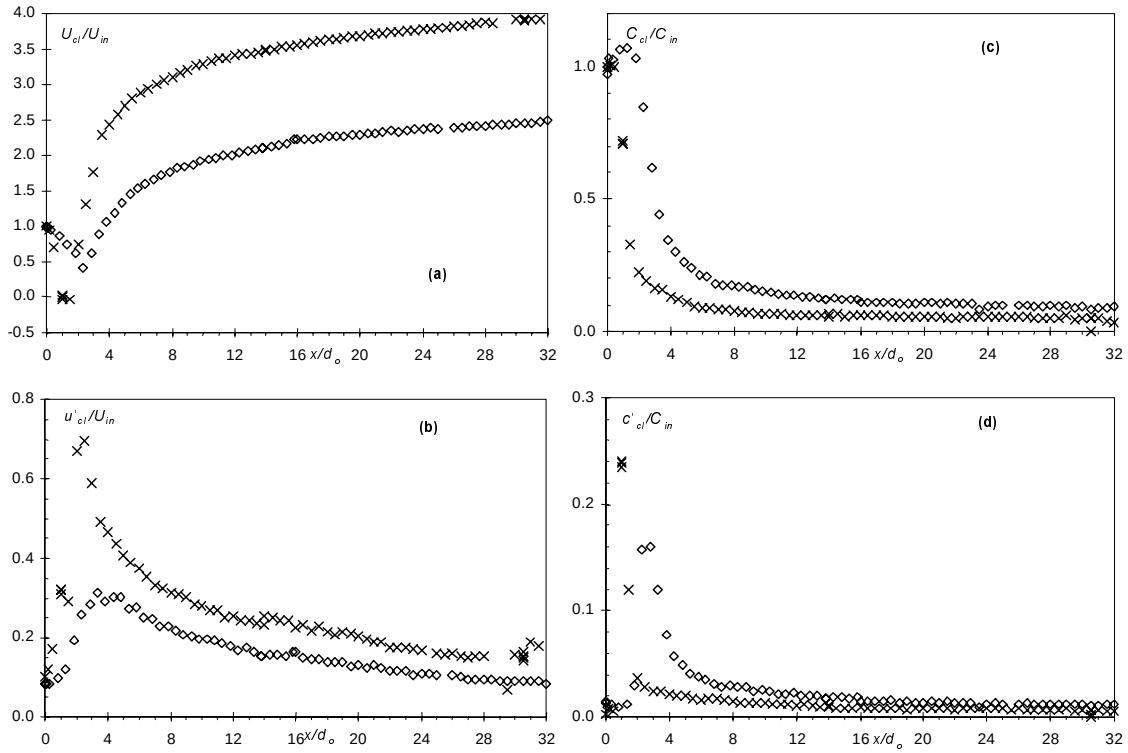


*Fig. 2. Mean axial velocity (a), turbulence intensity (b), mean concentration (c) and instantaneous concentration (d) along the centreline, for flow conditions 1 (◊) and 2 (×).*

Figure 2 shows the mean and instantaneous values of velocity and concentration along the tube axis. There is an initial region where the inner fluid decelerates, before being accelerated by the annular flow.

For experimental condition 1 ($U_a/U_{in}$ = 3.2) the minimum axial velocity is 0.4 $U_{in}$ at $x/d_0$ = 2.3, whereas in case of condition 2 ($U_a/U_{in}$ = 6.5), the deceleration can reduce the axial velocity to even negative values, at axial positions $x/d_0$ between 1 and 1.5. The occurrence of a backflow region for condition 2 agrees with the study by Rehab et al (1998), which indicates critical velocity ratio of 5.5 and 6.5 for diameter ratio $\beta = D/d_0$ of 1.37 and 2.29, above which recirculation may occur. In the present geometry, the diameter ratio $\beta$ was equal to 2.21 and the confinement apparently played no role in the onset of a region with axial negative velocity.

The location of the minimum velocity has been used as an indicator of the end of the inner potential core. This is a relatively important parameter, because the end of the inner potential core is also the end of the so-called initial merging zone (eg,, Ko and Au, 1981), or identically the end of entrainment of the inner jet by the co-flowing annular flow. The location of the minimum centreline velocity $x^u_{p1}$ (eg,, Ko and Au, 1981) and $x^u_{p2}$ the peak of the turbulence intensity (cf., Champagne and Wygnansky, 1971) have been the most commonly used parameters to determine the end of the merging zone. The latter gives rise to longer potential cores, at least in flow configurations with no backflow region, where the peak of turbulence intensity tends to occur already in the intermediate region, associated with the longitudinal acceleration of the flow.

The criteria above, however, are based on the flow hydrodynamic properties and two alternative indicators may be suggested, this time based on the scalar field: the location $x^c_{p3}$, where the mean concentration has dropped to 70% of its initial value, and $x^c_{p4}$, the location of the peak of the fluctuating concentration. The $x^c_{p3}$ criterion based on 70% of the mean concentration at the jet outlet, was set in accordance with the flow visualization, to be discussed in subsection 3.3. Table 2 summarizes the results of the utilization of these 4 criteria in the present flow conditions, and shows that all criteria are identical in case there is a recirculating flow region (condition 2), because that brings the inner flow potential core to a sudden end. If there is no backflow region, the criterion based on the minimum velocity seems to be the most appropriate

*Table 2. End of the inner flow potential core ($x/d_0$), as given by 4 different criteria (see text for details).*

| N. | $U_a/U_{in}$ | $x^u_{p1}$ | $x^u_{p2}$ | $x^c_{p3}$ | $x^c_{p4}$ |
|---|---|---|---|---|---|
| 1 | 3.2 | 2.3 | 4 | 2-2.5 | 3.2 |
| 2 | 6.5 | 1.0 | 1 | 1-1.5 | 1 |

Based on the minimum velocity criterion, the relationship between the inner potential core ($x_p$) and the velocity ratio was found to be,

$$\frac{x_p}{d_1} = \frac{8.98}{(U_a/U_{in})^{1.26}} \quad (1)$$

Rehab et al. (1998), for a geometry with non-confined coaxial jets, equates the potential core length according with the following relationship

$$\frac{x_p}{d_1} = \frac{A}{(U_a/U_{in})} \quad (2)$$

where A varies with the shape of the inner flow velocity profile at the inlet and the diameter ratio $\beta$. The parameter A increases with $\beta$, because a wider annular gap yields a larger potential core of the annular flow and hence the shear layer between flows reaches the axis further downstream. For geometries with identical $\beta$, A is higher for convergent geometries, in which case the inner flow has a uniform velocity profile and the flow rate is higher. Adjusting equation (2) to our work, we obtained A = 8.75 with a worse approximation to the experimental data, which was attributed to the effect of the confinement on the flow evolution.

For flow condition 1, the maximum axial turbulence intensity was 0.32 $U_{in}$, between $x/d_0$ = 3.3 and 5 in the flow accelerating region. This value exceeded by 2, the maximum axial turbulence intensity of 0.15 observed by Durão and Whitelaw (1973) in unconfined coaxial jets discharging into a quiescent ambient. In case of flow condition 2, two maxima, 0.32 $U_{in}$ and 0.7 $U_{in}$, were observed at $x/d_0$ = 1 and 2.5, associated, respectively with the end of the inner flow potential core and the maximum longitudinal gradient of the mean axial velocity (figure 3).

The sudden increase of velocity for $x/d_0 > 1$ and 2.5 causes a reduction of the mean concentration, which tends to approximately constant values at $x/d_0 = 10$ and 15, for flow conditions 2 and 1. The mean concentration decays at an identical rate, regardless of the velocity ratio; note that the differences between the two curves are a consequence of the different location of their maxima. Apparently, the instantaneous values of concentration, which can reach maximum values of 0.24 and 0.16 for conditions 2 and 1, are not influential in the decay of the mean concentration. The maximum concentration fluctuation occurs at the same longitudinal position where the mean axial velocity is minimum and the mean concentration shows a decrease approximately equal to 30% of its initial value. After this maximum of the concentration fluctuation, which occurs closer to the jet outlet for larger velocity ratio, there is a rapid decrease of the fluctuations.

## 3.2 Turbulent Mass Transport Field

### 3.2.1 Turbulent axial transport along the centreline

The maximum of longitudinal turbulent flux of mass (figure 3) is located at a distance $x/d_0 = 1$ and 2.3 from the jet outlet section, respectively for conditions 1 and 2. The peak of the turbulent flux, in case of condition 2, is twice as large, compared with condition 1.

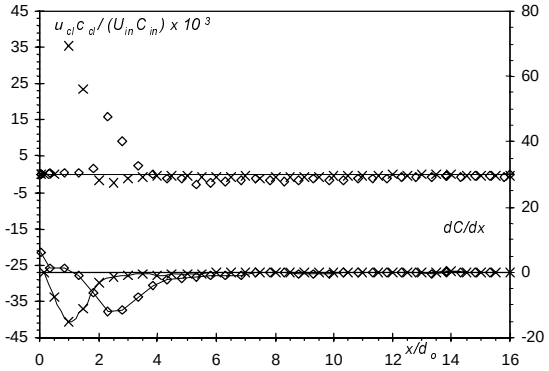


*Fig. 3. Turbulent axial transport and longitudinal gradient of mean concentration along the flow axis, for flow conditions 1 (◊) and 2 (×).*

Figure 3 also shows the longitudinal gradient of mean concentration, determined by numerical differentiation between consecutive data points. The location of the peak of $\partial C/\partial x$ (at $x/d_0 = 1$ and 2.3) coincides with the location of the maxima of the turbulent fluxes $uc$ mentioned above. These locations correspond also to the end of the inner potential core, as indicated by the criterion based on the minimum velocity (Table 2).

The turbulent flux of mass along the tube centreline is of gradient type, except in the intervals $2 < x/d_0 < 4$ and $4 < x/d_0 < 7$, in case of conditions 2 and 1, where the change of algebraic sign of $uc$ has no correspondence on the longitudinal gradient $\partial C/\partial x$ along the centreline. In either case, in those regions that correspond to the end of the inner potential core, the turbulent flux of mass is almost negligible and it may not preclude the utilization of gradient type models for prediction of the turbulent flux of scalar. Further downstream, for locations $x/d_0 > 4$ and $x/d_0 > 7$, in conditions 2 and 1, the turbulent flux is virtually zero, and turbulent longitudinal mixing becomes negligible.

### 3.2.2 Radial profiles of turbulent axial transport

The shape of the radial profiles of turbulent flux of mass (figures 5 and 6) are similar in conditions 1 and 2, apart from the profile at $x/d_0 = 1$, around the centreline. In case of condition 2 (the higher velocity ratio), this axial location corresponds to the beginning of the backflow region and that is the reason for the high values of the turbulent fluxes in the centreline (figure 6a) and high values of the instantaneous quantities $u$ and $c$, in figure 2b and 2d. The axial flux is positive around the centreline within a distance of less than 1 diameter from the outlet of the inner jet, for reasons that will become clear in subsection 3.4.

In order to assert whether the gradient diffusion also holds along the radius, the longitudinal gradient $\partial C/\partial x$ was plotted in figures 4 and 5. At first sight one would tend to conclude that gradient diffusion is valid, because the peaks of $uc$ and $\partial C/\partial x$ occur at identical radial locations. There are, however, other aspects that reveal the non-gradient nature of the axial turbulent flux of the passive scalar, namely the change of algebraic of $uc$ in the inner region in case of the radial profiles at $x/d_0 = 1$ and the high values $\partial C/\partial x$ at $x/d_0 = 4$, a location where $uc$ goes to zero.

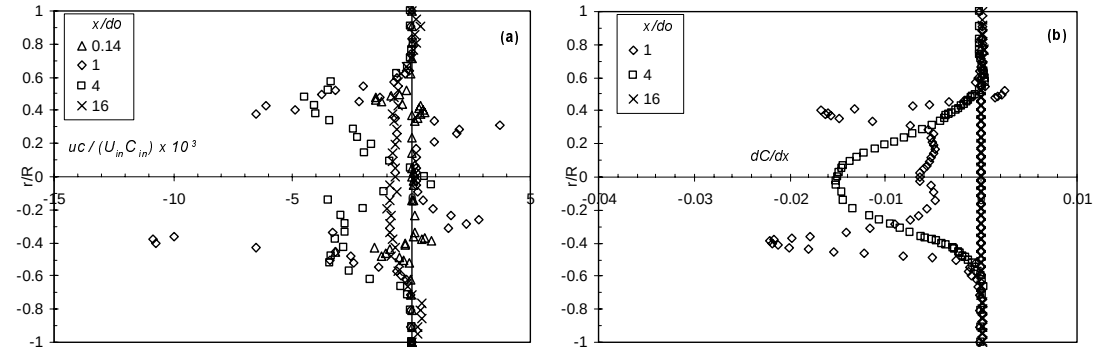


*Fig. 4. Radial profiles of (a) axial turbulent transport and (b) longitudinal gradient of mean concentration, for flow condition 1.*

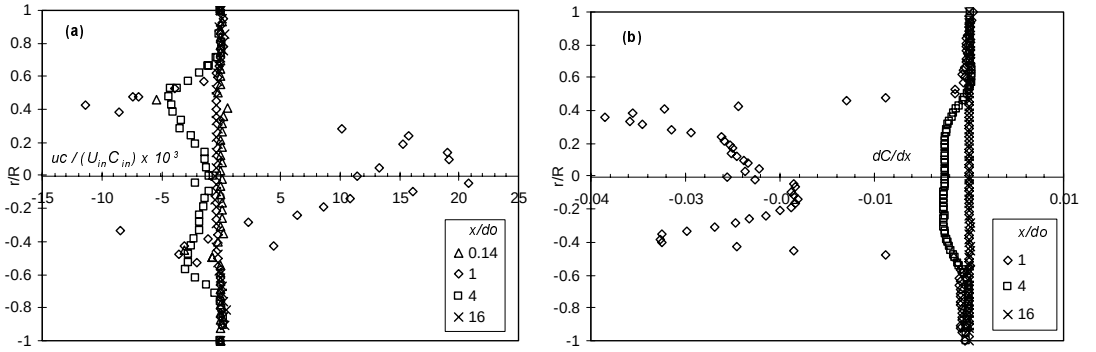


*Fig. 5. Radial profiles of (a) axial turbulent transport and (b) longitudinal gradient of mean concentration, for flow condition 2.*

For flow condition 2 (figure 5), the radial profiles of turbulent axial transport are qualitatively identical and the analysis above also applies.

### 3.2.3 Radial turbulent transport

The radial turbulent mass transport $vc$ (figures 6 and 7) is lower than the axial turbulent mass transport (figures 4 and 5), although radial gradients are 10× higher than longitudinal gradients of concentration. This was observed also by Johnson and Bennett (1984), and apart from a poor correlation between the derivatives of the mean concentration field and the turbulent flux of the scalar quantity, also evidences a high anisotropy of the turbulent diffusion. Radial transport is low for $x/d_0 = 0.14$ and 1, most likely due to the spatial resolution of the measuring system, since the control volume is larger than the whole spatial region where $\partial C/\partial r$ is different from zero. In the majority of the profiles $vc$ is positive or null, and in agreement with the radial gradient of concentration.

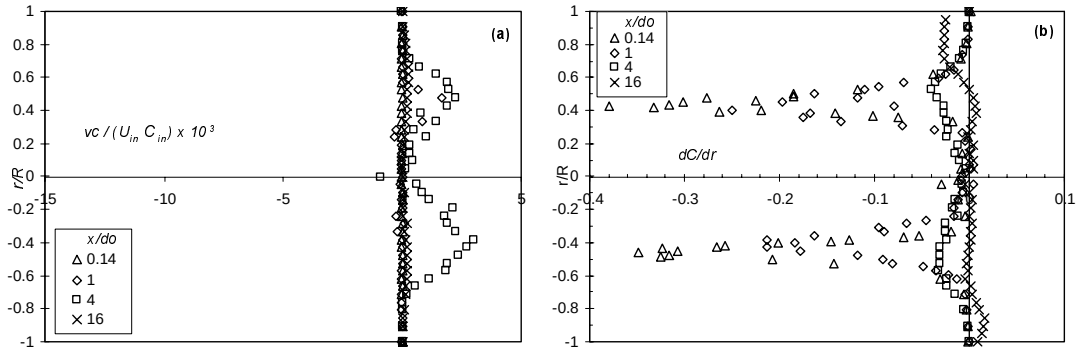


*Fig. 6. Radial profiles of (a) radial turbulent transport and (b) radial gradient of mean concentration, for flow condition 1.*

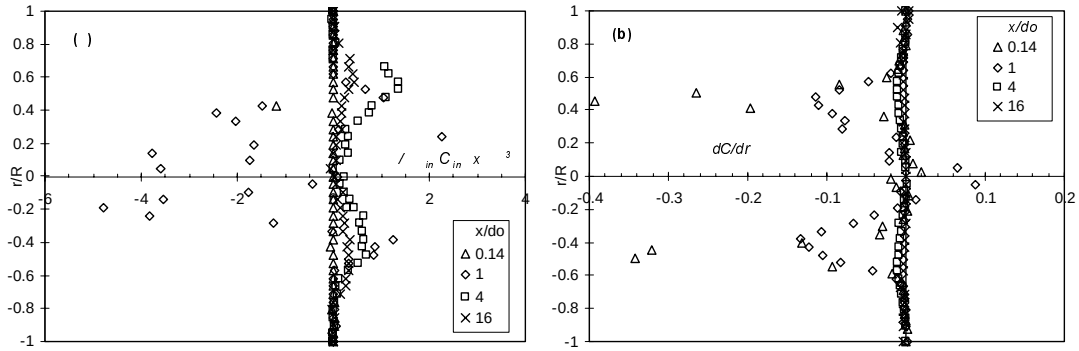


*Fig. 7. Radial profiles of (a) radial turbulent transport and (b) radial gradient of mean concentration for flow condition 2.*

### 3.3 Flow Visualization

The flow visualization (figure 8) comprised the first 2 diameters $D$ (about 4 inner jet diameters $d_0$ long), where most of the flow changes took place. A mixture of water and high concentration rhodamine was injected trough the inner tube, to observe the flow structure and the mixing between the annular and the inner flows. There are two images (still images averaged over 125 μs) per experimental condition, to illustrate the turbulent nature of the flow, particularly in the mixing layer between the inner and the annular flow.

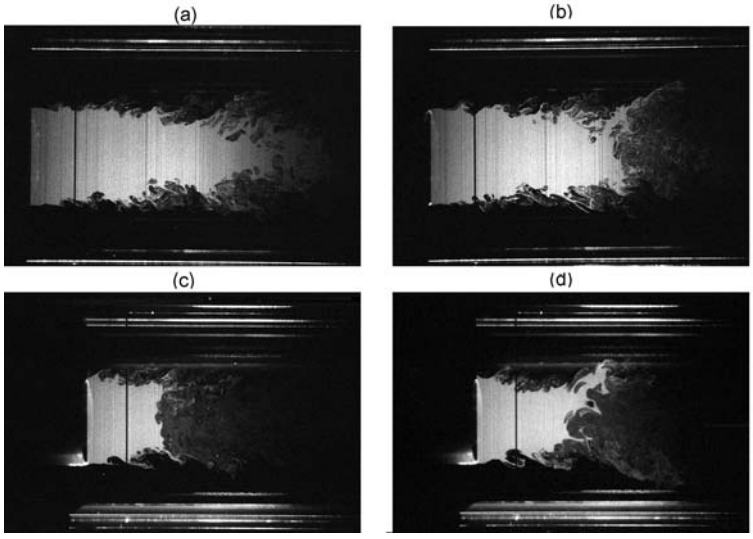


*Fig. 8. Flow visualization for flow conditions 1 (figs a and b) and 2 (figs c and d)*

In average terms, different flow regions can be identified in figure 8, in accordance with the published literature on coaxial jet flows (eg, Ko and Au, 1981), as the flow evolved from two individual coaxial fluxes to the classic turbulent flow inside a tube, with a uniform radial mean concentration distribution. The images allow the identification of the potential core, whose end coincides with axial positions where the mean concentration dropped to about 70% of its initial value (Dahm, 1992), resulting in the $x^c_{p3}$ criterion (Table 2, subsection 3.1). In figure 8a the conical shear layer reaches the tube axis at $x/d_0 = 3$, whereas in figure 8b these happens earlier and lower size eddies, made of non mixed inner fluid, are observed after the disappearance of the inner jet core.

The shear layer between the inner and annular flows is the region of main interest. The higher turbulence intensity of condition 2, compared with condition 1 is supported by figures 8c and 8d, which compared with frames 8a and 8b, display a more erratic pattern and larger flow structures, both along the tube centreline and in positions halfway between the tube wall and the axis. This is also explained by the earlier disappearance of the inner jet core at $x/d_0 = 1$ and the occurrence of recirculation in condition 2. These images are identical to those of Rehab et al. (1997), who identifies a recirculation bubble for a velocity ratio $U_a/U_{in} = 15$. In figures 8c and 8d, the recirculation bubble occurred between $x/d_0 = 1$ and 2, with an average length identical to the inner jet diameter $d_1$.

## 3.4 Probability Density Functions and Higher Order Moments

Skewness $S$ and flatness $F$ different from 0 and 3 are an indication of departure from Gaussian probability distribution, which is the asymptotic state of a well-mixed solution. See for instance figures 9 and 10 for radial profiles of $S$ and $F$ at $x/d_0 = 16$, where the mean concentration radial profiles were almost uniform and probability density functions are symmetrical, with skewness and flatness close to their Gaussian values. $S$ and $F$ are also indicators of the flow intermittency, usually associated with the presence of a wider range of length scales.

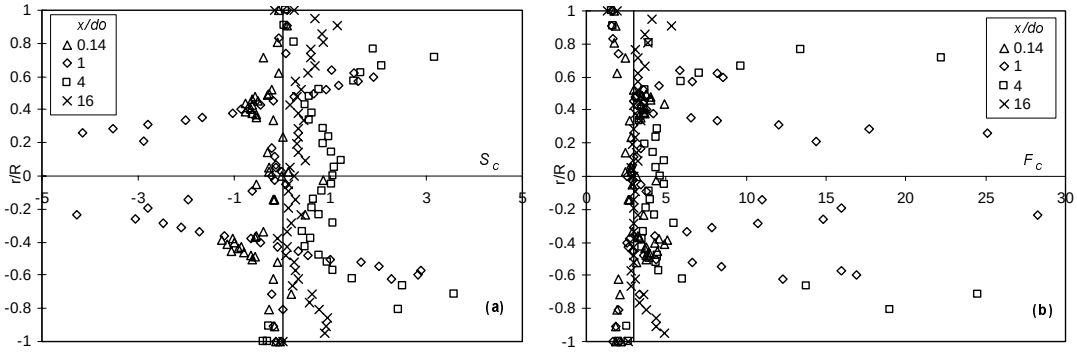


*Fig. 9. Radial profiles of skewness (a) and flatness (b) of concentration distributions, for flow condition 1.*

If one excludes the axial location $x/d_0 = 1$, the shape of the radial profiles of $S$ and $F$ are identical, regardless of the velocity ratio. This is not surprising, because the mean flow pattern is identical. Skewness and flatness are generally higher (see profiles at $x/d_0 = 1$ and 4) in condition 1 than in condition 2, confirming the higher mixing rates achieved by condition 2, because of its higher velocity ratio, 6.5 compared with 3.2 in condition 1.

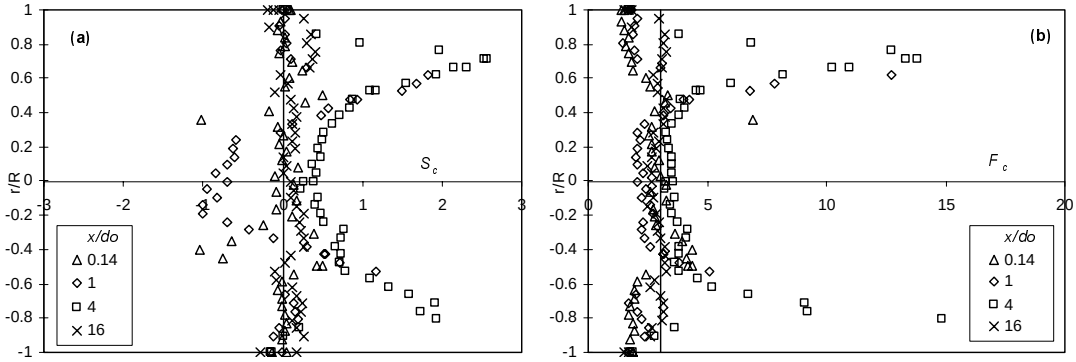


*Fig. 10. Radial profiles of skewness (a) and flatness (b) of concentration distributions for flow condition 2*

The axial location $x/d_0$ = 1, however, is different and constitutes a particular case, because if in condition 1, the radial profile goes through the core of the inner flow, which will end by $x/d_0$ = 2.3 (Table 2), in condition 2, the location $x/d_0$ = 1 corresponds to the end of core of the inner flow, which is also the location of one of the free stagnation points of the recirculation region. This explains the two peaks of *F* in each side of the centreline in condition 1, at distances around *r/R* equal to 0.7 and 0.2. Condition 2, on the other hand displays one single peak at a distance *r/R* = 0.6, and a well-mixed region in a wider area around the centreline, with *F* and *S*, close to their Gaussian values of 3 and 0.

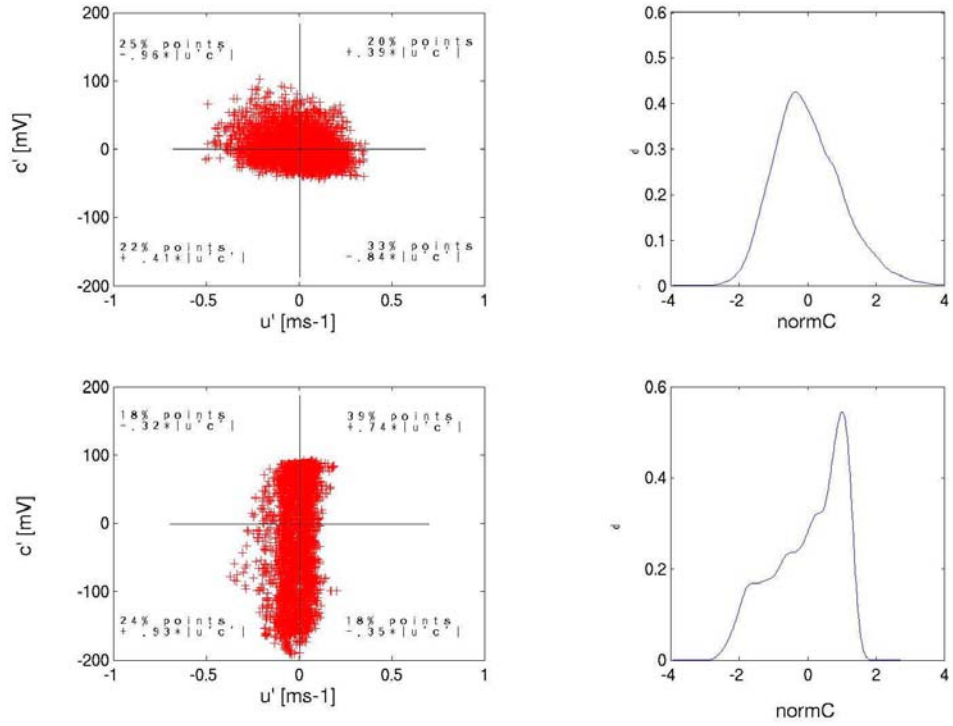


*Fig. 11. PDFs of fluctuating concentrations and scatter plots of velocity and scalar contributions to the axial turbulent flux of mass, for condition 2, at $x/d_0$ = 1 and two radial locations (a), first row, in the shear layer between the two co-flows at r/R = 0.48; and (b) second row, around the centreline, at r/R = 0.19.*

Figure 11 displays the joint instantaneous values of axial velocity and concentration in quadrants, enabling a more detailed analysis of the fluid mixing process, in a manner used for identification of organized structures in boundary layer flows by, for instance Willmarth and Lu (1972), Kim et al (1987) or Katul et al (1996). Four different contributions can occur to the turbulent flux *uc*, depending on the algebraic signs of *u* and *c*. If we consider the concentration as a tag of the inner jet fluid, contributions from the upper half of the diagram (quadrants 1 and 2, where $c > 0$) are associated with the inner fluid, whereas the lower half of the diagram (quadrants 3 and 4, where $c < 0$) may be associated with the annular fluid. The radial profiles of *c* and *u*, from Lima (2000) and not included in the present work, showed that the radial profile of the fluctuating concentration develops in a bell-like shape with a maximum on the centreline, whereas the fluctuating velocity is maximum on the jets shear layer at around *r/R* = 0.5 and again close to the tube wall. If high fluctuations of the concentration can undoubtedly be associated to the inner jet fluid, at $x/d_0$ = = 1 there is no clear way of telling whether high *u* is associated with annular or inner jet fluid, since it may have contributions of both. Surely, high fluctuating *u* fluid originated from the shear layer, a region of relatively low concentration.

The two radial locations, in figure 11, are associated with negative and positive axial flux *uc*, at *r/R* = 0.48 and 0.19, the first and second rows (see also figure 5, for the radial profile and algebraic signs of *uc)*. In case of the location close to the centreline, *r/R* = 0.19, the axial flux *uc* is made of contributions from the first and third quadrants, which we interpret, in the case of the first quadrant, as made mainly of inner jet fluid (high concentration) accelerated by the annular fluid, or trapped into eddies of annular flow that travelled radially inward; or in case of the third quadrant, initially annular fluid that transferred momentum into neighbouring inner jet fluid. Contributions in the first and third quadrant are likely associated with respectively the acceleration of the inner fluid by the co-flowing annular flow, and the

reverse, i.e. the deceleration of the annular flow by the lower velocity fluid originated from inner radial locations. The net contribution of the four quadrants is positive and we may conclude that the mixing process described dominated compared to what occurred at locations radially outward as described below.

At $r/R$ = 0.48 the net contribution of the four quadrants is negative, as a result of products $u < 0$ times $c > 0$ (second quadrant) and products $u > 0$ times $c < 0$ (forth quadrant) and we interpreted the mixing process at this location as made up mainly of individual pockets of what was initially inner and annular jet fluid.

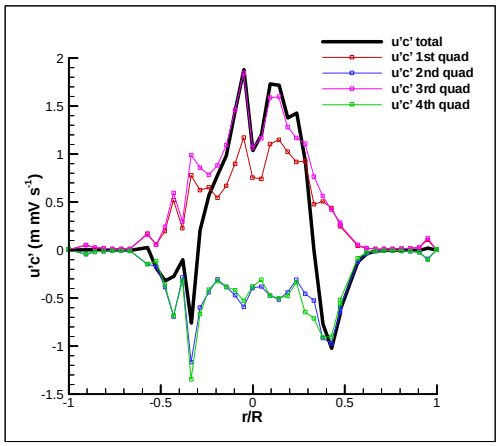


*Fig. 12. Quadrant analysis of axial turbulent flux of mass, for condition 2, at $x/d_0 = 1$.*

For a global view of the turbulent diffusion, we show in figures 12 and 13, the contributions of all 4 quadrants across the radius at 2 axial locations $x/d_0$ = 1and 4. The positive flux of *uc* occurs only at $x/d_0 = 1$ and in a region around the centreline at radial distances of less than 0.3*R.* Contributions from the second and forth quadrant are the most frequent and explain the negative fluxes of *uc.*

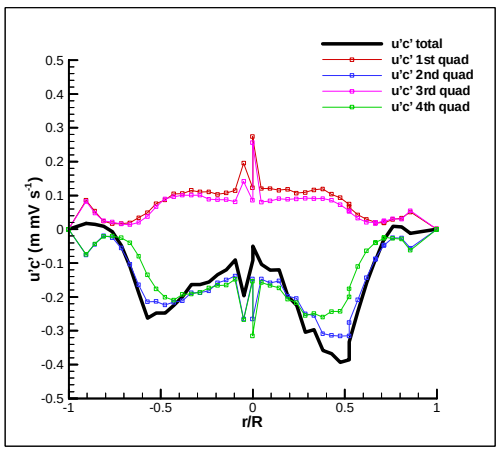


*Fig. 13. Quadrant analysis of axial turbulent flux of mass, for condition 2, at $x/d_0 = 4$.*

## 4. CONCLUSIONS

Simultaneous velocity and concentration measurements, by joint LDV/LIF techniques, were made on coaxial confined jets of velocity ratios $U_a/U_{in}$ = 3.2 and 6.5, to illustrate the mixing process of a passive scalar, in high Reynolds number flows. The main conclusions can be summarized as follows:

1. For lower velocity ratio (3.2) the minimum axial velocity was 0.4 $U_{in}$ at $x/d_0$ = 2.3, whereas in case of higher velocity ratio (6.5), the deceleration reduced the axial velocity to even negative values, at axial positions $x/d_0$ between 1 and 1.5.

2. The occurrence of this backflow region agreed with previous studies in non-confined flows and apparently, the confinement played no role in the onset of a region with axial negative velocity.

3. In case of backflow, axial turbulence intensity exhibited 2 peak values, at the location where the axial velocity reached its minimum and where the longitudinal gradient of axial velocity was larger. In this case also, the peak of the turbulent flux *uc* more than doubled the turbulent flux *uc*, associated with the experimental condition 1, with a lower velocity ratio and no centreline recirculation.

4. The increase in mean axial velocity causes the decrease of mean concentration at the flow axis, with the instantaneous concentration fluctuation maximum being observed at the same longitudinal position where mean axial velocity was minimum and the mean concentration had been reduced to a value equal to 0.7 $C_{in}$.

5. Radial turbulent mass transport was in accordance with gradient-transport methods, however, counter-gradient axial mass transport prevailed in the flow inner region of the flow, after the disappearance of the inner core.

6. Quadrant analysis showed that the negative axial turbulent flux *uc* was restricted to a region around the centreline, after the end of the inner core.

**Acknowledgments**

This experimental work was performed in the Hydraulics Laboratory of the Civil Engineering Department of the Faculty of Engineering of the University of Porto. The technical support of Mr. Jerónimo Sousa and the friendly interest of Dr. Fernanda Proença are gratefully acknowledged. The study is based in part on the doctoral thesis of the first author, under grants BD/2033/92/RN and BD/5623/95 of programmes *Ciência* and *Praxis XXI*, and was developed under research contract PEAM/C/APR/132/91, entitled *Dispersion Studies in Liquid Flows by Laser Induced Fluorescence*, and more recently also under project POCTI/33980, *BULET - Boundary Layer Effects and Turbulence in Complex Terrain*, all funded by the Portuguese Foundation for Science and Technology (FCT).

**REFERENCES**

Arcoumanis, C., McGuirk, J.J. and Palma, J.M.L.M. (1990). "On the use of fluorescent dyes for concentration measurements in water flows", Experiments in Fluids, **10**, pp. 177-180.

Bradshaw, P. (1994). "Turbulence: The chief outstanding difficulty of our subject", Experiment in Fluids, 16, pp. 203-216.

Champagne, F.H. and Wygnansky, I.J. (1971). "An experimental investigation of coaxial turbulent jets", Int. J. Heat Mass Transfer, 14, pp.1445-1464.

Dahm, W.A., Friedler, C.E. and Tryggvason, G. (1992). "Vortex structure and dynamics in the near filed of a coaxial jet", Journal of Fluid Mechanics, 241, pp. 371-402.

Durão, D. and Whitelaw, J.H. (1973). "Turbulent mixing in the developing region of coaxial jets", Transactions of the ASME-Journal of Fluids Engineering, pp. 467-473.

Johnson, B.V. and Bennett, J.C. (1981). "Mass and momentum transport experiments with confined coaxial jets", Technical Report NASA-CR-165574 and UTRC report R81-915540-9.

Johnson, B.V. and Bennett, J.C. (1984). "Statistical characteristics of velocity, concentration, mass transport and momentum transport for coaxial jet mixing in a confined duct", Journal of Engineering for Gas Turbines and Power, 106, pp. 121-127

Katul, G., Kuhn, G. Schieldge, J. and Hsieh, C.-I. (1996). "The ejection-sweep character of scalar fluxes in the unstable surface layer", Boundary-Layer Meteorology, 83, pp. 1-26.

Kim, J., Moin, P. and Moser, R. (1987). "Turbulence statistics in fully developed channel flow at low Reynolds number", Journal of Fluid Mechanics, 177, pp. 133-166.

Ko, N.W.M. and Au, H. (1981). "Initial region of subsonic coaxial jets of high mean-velocity ratio", Journal of Fluids Engineering, 103, pp. 335-338.

Lima, M.M.C.L. (2000). “Simultaneous Measurement of Velocity and Concentration by Laser Doppler Anemometry and Laser Induced Fluorescence” (*in Portuguese*), PhD Thesis, University of Porto.

Lima, M.M.C.L., Palma, J.M.L.M. and Areal, P.M. (2002). “Scalar Measurements by Laser Induced Fluorescence”. In Proceedings of 11th International. Symposium on Applications of Laser Techniques to Fluid Mechanics, 8-11 July, Lisbon, Portugal. Session 27, entitled *LIF for Scalar Measurements.*

Rehab, H., Villermaux, E. and Hopfinger, E.J. (1997). “Flow regimes of large-velocity-ratio coaxial jets”, Journal of Fluid Mechanics, 345, pp. 357-381.

Rehab, H., Villermaux, E. and Hopfinger, E.J. (1998). “Geometrical effects on the near-field structure of coaxial jets”, AIAA Journal, 36(5), pp. 867-869.

Villermaux, E. and Rehab, H. (2000). “Mixing in coaxial jets”, Journal of Fluid Mechanics, 425, pp. 161-185.

Willmarth, W.W. and Lu, S.S. (1972). “Structure of the Reynolds stress near the wall”, Journal of Fluid Mechanics, 55 pp. 65-92.